An RNN-LSTM Enhanced Compact and Affordable Micro Force Sensing System for Interventional Continuum Robots With Interchangeable End-Effector Instruments

Shilong Yao, Ruijie Tang, Long Bai, Hong Yan, *Fellow, IEEE*, Hongliang Ren, *Senior Member, IEEE*, and Li Liu, *Member, IEEE*

***Abstract*— Micro force sensing in various clinical scenarios is a challenging issue to be addressed. It is highly difficult to trade off the size, cost, and measurement accuracy of a micro force sensing system. In this article, a compact and affordable micro force sensing system enhanced by deep neural network is proposed. A three-axis force sensor is designed and fabricated with a footprint of only 14 mm and is employed to transform the force on the material structure into more accurate distance information. Such a sensor configuration can be seamlessly interfaced with the distal end of our in-house compliant and flexible continuum robot. On top of that, the RNN-LSTM network is exploited to augment the micro force sensing capability of the distal end-effector of the robot, which addresses the limitation on the nonlinear force issue of the continuum robot and the material itself. The RNN-LSTM network alone can be employed to perform force curve fitting for specific interventional tasks. The results indicate that more than 90% accuracy has been achieved, and the network can be applied to large-scale continuum robot-assisted interventional scenario deployment and teleoperation force perception.**

Manuscript received 16 January 2023; revised 16 April 2023; accepted 30 May 2023. Date of publication 22 June 2023; date of current version 17 July 2023. This work was supported in part by the Shenzhen Key Laboratory of Robotics Perception and Intelligence under Grant ZDSYS20200810171800001; in part by the Southern University of Science and Technology, Shenzhen, China; in part by the Hong Kong Research Grants Council (RGC) Collaborative Research Fund under Grant CRF C4026-21GF and Grant CRF C4063-18G, in part by the General Research Fund under Grant GRF #14211420, Grant GRF #14220622, and Grant GRF #14204321; in part by CUHK-Direct Grant 134997202 and Project CityU 9610034; in part by the Shun Hing Institute of Advanced Engineering at the CUHK under Grant BMEp1-21/8115064; and in part by the Shenzhen–Hong Kong–Macau Technology Research Programme (Type C) under Grant 202108233000303. The Associate Editor coordinating the review process was Dr. Anoop Chandrika Sreekantan. *(Shilong Yao and Ruijie Tang are co-first authors.) (Corresponding authors: Li Liu; Hongliang Ren.)*

Shilong Yao is with the Shenzhen Key Laboratory of Robotics Perception and Intelligence and the Department of Electronic and Electrical Engineering, Southern University of Science and Technology, Shenzhen 518055, China, and also with the Department of Electrical Engineering, City University of Hong Kong, Hong Kong, SAR, China (e-mail: shilong.yao@my.cityu.edu.hk).

Ruijie Tang, Long Bai, and Li Liu are with the Department of Electronic Engineering, The Chinese University of Hong Kong, Hong Kong, SAR, China (e-mail: ruijie.tang@link.cuhk.edu.hk; b.long@ieee.org; liliu@cuhk.edu.hk).

Hong Yan is with the Department of Electrical Engineering, City University of Hong Kong, Hong Kong, SAR, China (e-mail: h.yan@cityu.edu.hk).

Hongliang Ren is with the Department of Electronic Engineering and the Shun Hing Institute of Advanced Engineering, The Chinese University of Hong Kong, Hong Kong, SAR, China, also with the Department of Biomedical Engineering, National University of Singapore (NUS), Singapore 117575, and also with the NUS (Suzhou) Research Institute, Suzhou 215123, China (e-mail: hlren@ieee.org).

Digital Object Identifier 10.1109/TIM.2023.3288245

***Index Terms*— Continuum robot, deep neural network, interchangeable instrument, micro force sensor, soft sensor.**

I. Introduction

MEDICAL robots with their applications have demonstrated international significance in the robotics research community [1]. To maintain operation safety, contact force sensing functionality is crucial for the surgical or interventional robotic system. The kinds of literature have revealed that the loss of force sensing and feedback can be highly difficult for physicians/surgeons to perform robot-assisted procedures via teleoperation precisely. Typical examples include oropharyngeal/nasopharyngeal swab robot [2], [3], robot-assisted bronchoscopy [4], robot-assisted cardiac interventions [5], and needle insertion for robot-assisted eye surgery [6]. Among them, nonlinear elements exist such as tool–tissue interaction, continuum, and soft mechanical structures, and elasticity of soft tools in the medical robotics system when the interventional tasks are performed [7], [8], [9]. These factors may make micro force sensing at the distal end of continuum robots difficult to predict in various interventional applications.

With the development of machine learning, it is inherently suited for such flexible and soft robotic systems in which the dynamics are complex and implicit governing equations can manage the tip forces [10]. A flexible micro 6-D force sensor with tendon-and-mortise structure utilizes a deep neural network to sense the force for orthodontics treatment with linear error to be 0.008 N [11]. To achieve the nonlinear mapping relationship between magnetic field information and contact force, an LSTM model is used to train the perception ability of the soft magnetic fingertip [12]. Without an additional force sensor mounted on surgical instruments, Guo et al. [13] provided a lightweight deep neural network to achieve high-accuracy grip force measurement. Machine learning methods have been deployed in soft tactile sensing for contact localization and force prediction to overcome the limitations. Both the kinematic and force modeling of soft actuators are achieved by incorporating embedded flexible sensors and the recurrent neural network (RNN) [14]. In addition, by avoiding using direct measurements from the force sensor,

Wan et al. [15] proposed a visual learning method to estimate the 6-D force and moments toward a variety of stiffness. Although deploying various machine learning techniques in soft robotic systems demonstrates promising results in force sensing, there are still unresolved challenges. Overfitting as a fundamental concern in machine learning may be serious for force sensor calibration since the calibration process requires strict forces or moments applied along x-, y-, and z-directions. This can cause the forces sensor loss of generality when inferences occur, such as tool–tissue interaction and distance variations during interactions. Moreover, there is a lack of comparison studies among a variety of machine learning approaches toward some specific application scenarios. The merits of different algorithms deployed in specific applications require further demonstration and interpretation.

In recent years, continuum robotics have been broadly adopted in robot-assisted interventions involving intubation, suture, and medicine administration in vivo due to their high dexterity and mobility. In general, indirect estimation of the proximal model and direct measurement of the distal force sensor are two ways to sense the distal force of surgical robots. Various researchers have explored the perception of surgical interaction force by using proximal sensing data and kinematic models. They have already achieved the measurement of the distal end force value of the continuum body based on the length of the external rope and the tensile force [16], the extended Kalman filter (EKF) to estimate the distal end force through the overall shape [17], and incorporating the curvature of the catheter with the kinematic model to estimate the distal end force [18]. However, these techniques usually require integrating complex and high-cost sensing systems. To sense the contact force at the distal end of the continuum robots can provide straightforward feedback for operators or autonomous robotic systems. Miniature sensors such as the embedded fiber Bragg grating (FBG) have been deployed to address the force sensing issues; while the end-effector instrument is replaced and adapted to different clinical purposes, it may be challenging to apply the calibrated micro force sensor to perform different interventional tasks [19], [20], [21], [22]. Besides, researchers have tried to use deep neural networks to estimate the distal end force of the continuum robot. Among them, an RNN-based tip force estimator was developed for the continuum manipulator and its performance was listed to be compared with the multi-layer perception method and build-in static model [23].

Overall, we need to address the limitation of the loss of generality in machine learning-based force sensing calibration. Specifically, the generality indicates that for different interventional tasks, our proposed system and method can still fulfill high-accuracy micro force sensing based on a pretrained neural network model. Our strategy is that the different neural networks are trained for different interventional tasks. Additional collected sensing data are used to validate our network toward the specific interventional task. Besides, the majority of rigid robotic system possesses the merit of tip force sensing with high accuracy since the associated modeling can be explicitly represented. We need to provide the same function for the continuum/soft robotic system, which requires its compact design distally integrating with the robot, and compatibility with different end-effector instruments.

In this article, a novel micro force sensing system is developed. The contributions are mainly associated with the following three aspects.

1) We designed and fabricated a compact and affordable micro force sensing system distally integrated with an in-house continuum robot platform. Such a design can achieve sensing and gripping functions with high safety and flexibility and holds the advantages of low cost and is easy to fabricate.
2) We proposed an augmented force sensing approach based on deep neural networks for specific interventional tasks.[1] The complex modeling of continuum and soft mechanisms as well as trivial calibration procedure is not required. Specifically, by comparing the performance among a variety of neural networks, the LSTM-RNN network is chosen and deployed to carry out validation experiments.
3) We evaluated the system efficacy for four typical continuum robot-assisted interventional procedures including swabbing, needle insertion, microneedle insertion, and palpation. For the respective task, the interventional continuum robot can fulfill mode-switching to obtain achieve force sensing and identify different stages of procedure enhanced by the pretrained neural networks.

II. Design and Implementation

The compact and affordable micro force sensing system is designed to measure the 3-D forces and fabricated to conduct delicate tasks such as oropharyngeal swab sampling, needle insertion, and in vivo palpation. The proposed force-sensing tip contains an optoelectronic sensor circuit board and a soft tool gripper (see Fig. 1).

A. Continuum Robot Design

The continuum robot described in this article is made up of Nitinol wires, a shape memory alloy material with a high strength of 895 MPa, and multiple 3-D-printed disks made of poly-lactic acid (PLA) with a diameter of 8 mm. The material's consistent force provides durability and is ideal for long-term medical applications. All parts of the system are 3-D printed, including the disk, which has an inner diameter of 1.0 mm and an outer diameter of 8 mm. The disk also contains four evenly spaced holes with a diameter of 0.35 mm along the radial direction, with a distance of 2.5 mm between them. Dyneema lines with a diameter of 0.32 mm are then evenly distributed along the axial direction.

To achieve deflection, two wires of the same diameter are connected to an MG996R motor. In addition, the PCB board at the base of the robot has four 0.5 mm holes for the wires to pass through, ensuring consistent tension and relative positioning between the sensor and the end of the continuum robot for standardized assembly and deployment

[1]Official implementation at: github.com/ShilongYao0114/An-RNN-LSTM-Enhanced-Force-Sensing-System.

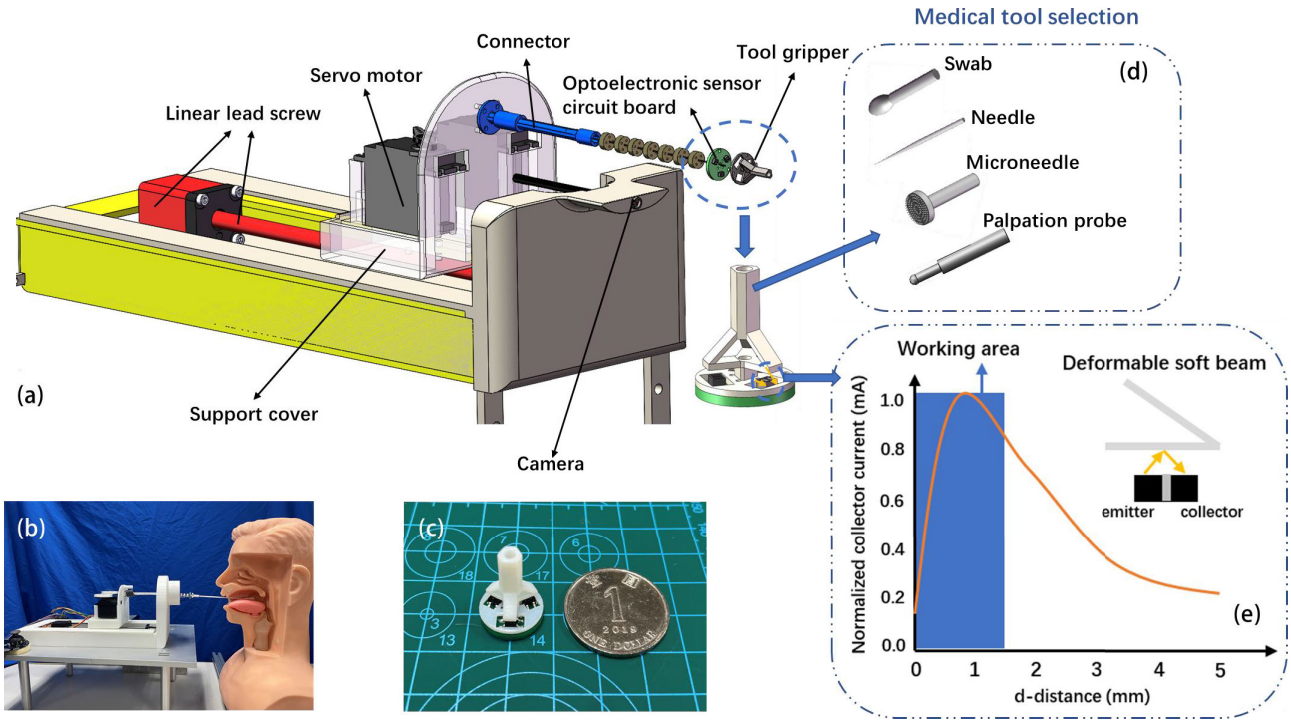

Fig. 1. (a) Overall system design. (b) Theoretical application scenarios. (c) Sensor size compared with the coin. (d) Desired four different medical tools. (e) Current performance with the distance change.

of neural networks for long-term use. The printed disks are spaced at 8 mm and evenly distributed, with instant adhesive (Ergo 5210) used to fix the disks and Nitinol wires in place. After 30 min of curing time, the Dyneema wire can pass through the 0.35 mm hole of the disks in the axial direction. The PCB and 3-D-printed soft gripper can be prefixed using 2-mm bolts. The other end of the Dyneema wire is wound and fixed with the turning disk installed on the MG996R steering gear using bolts (M1.6). This assembly method ensures the pulling force of the Dyneema line and the force applied to the continuum robot are consistent, with adjustable length and tension. In addition, the bottom of the continuum robot is fixed to a linear slider (CTM-28), which provides the robotics system with an extra degree of freedom with a maximum moving range of 150 mm. The entire robot system is manufactured using only two motors and simple 3-D-printed parts with a self-designed circuit board, allowing for low-cost, large-scale deployment in medical scenarios thanks to the standardization of the manufacturing process and consistency of the parts.

According to the geometric relation of the continuum robot, each segment of the continuum robot is evenly distributed, and each disk has the same spacing distance. Then, the two wires are always in tension. Therefore, we can use the constant curvature model to calculate its workspace. The kinematic model of the continuum robot with a single-joint segment is shown in Fig. 2(a). It is simplified as a continuous smooth curve of equal curvature. Three key variables of continuum robots are defined as continuum robot length L_1, bending angle θ, and rotation angle φ, which are the parameters between plane $x_0y_0z_0$ and plane $x_1y_1z_1$. As the wire diameter between each disk used is 8 mm, the distance of the continuum robot part and the force sensor height is $L_1 = 80$ mm and $L_2 = 20$ mm, respectively. The d represents the slider distance. So,

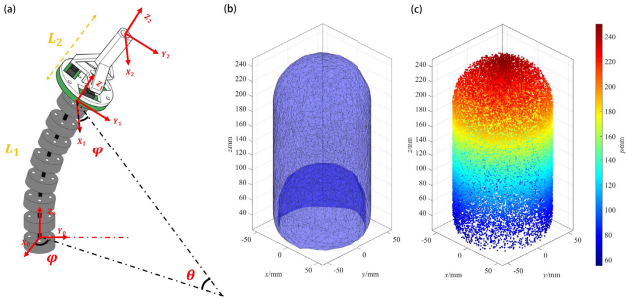

Fig. 2. (a) Continuum robot kinematic model diagram. (b) and (c) Robot working space implementation.

the conversion matrix T_i can be written as

$$T_i = \text{Trans}(L)R_Z(\varphi_i)R_Y(\theta_i)R_Z(-\varphi_i) = \begin{bmatrix} R_i & P_i \\ 0 & 1 \end{bmatrix} \quad (1)$$

where T_i represents the translation matrix, and R_Z, R_Y, and R_Z represent the coordinate transformation matrix around $+x$, $+y$, and $+z$, respectively. R_i is the rotation matrix, which is a 3 by 3 matrix, and can be expressed by (2). P_i is the position vector, which is a 3 by 1 matrix, and can be expressed by (3)

$$R_i = \begin{bmatrix} c\theta_i c^2\varphi_i + s^2\varphi_i & c\theta_i c\varphi_i s\varphi_i - c\varphi_i s\varphi_i & s\theta_i c\varphi_i \\ c\theta_i c\varphi_i s\varphi_i - c\varphi_i s\varphi_i & c^2\varphi_i + s^2\varphi_i c\theta_i & s\theta_i s\varphi_i \\ -s\varphi_i c\varphi_i & -s\theta_i s\varphi_i & c\theta_i \end{bmatrix} \quad (2)$$

$$P_i = \begin{bmatrix} \frac{L_1}{\theta_i}\cos(\varphi_i(1-c\theta_i)) & \frac{L_1}{\theta_i}\sin(\varphi_i(1-c\theta_i)) \\ \frac{L_1}{\theta_i}\sin(\theta_i) + L_2 + d \end{bmatrix}^{\mathrm{T}}. \quad (3)$$

TABLE I
COST OF THE FORCE SENSING AND ROBOTIC SYSTEM

Structure	Type	Quantities	Cost
Optoelectronic sensor	QRE1113	3	$2
Soft gripper	TPU95A 3D-printed	10g	$4.6
PCB	Self-designed	1	$1
Force sensing system			Total $7.6
Controller	Arduino Mega 2560	1	$10
Joystick	X2K4P2	1	$3
Linear slider	CTM28-150	1	$6
Servo motor	MG996R	2	$6
Supporting components	PLA 3D-printed	500g	$50
Continuum robot			Total $75

After obtaining the above transformation matrix and its parameter relationship, we can deduce the working space of the system according to the sliding stage length d and the continuum robot length L_1 and use the Monte-Carlo method to capture the overall motion space. According to Fig. 2(b) and (c), the total workspace area can achieve approximately $51 \times 51 \times 250$ mm^2.

B. Micro Force Sensor Design

To create the base of the force sensor, a PCB board with a diameter of 14 mm and a thickness of 1.5 mm was designed. Three optoelectronic sensors were evenly distributed with a radius of 6 mm on the top side. The bottom side of the board has holes for wiring, ensuring the 3-D-printed gripper and the PCB board fit tightly. For the gripper design, a tripod-shaped structure was proposed to perform both force sensing and tool gripping. Force sensors of varying thickness (1, 1.5, and 2 mm) were designed and printed using thermoplastic polyurethanes (TPU) with a Shore hardness of 95 A and a flexural modulus of 78.7 MPa, which deflects easily under a small pressure. Due to the inherent compliance of the material, it cannot be damaged when the external force exceeds the predefined limit. After up to 1000 bending tests shown in Fig. 3(c), the sensor maintains good rebounding and recovery performance, while the optoelectronic sensor readings remain consistent even when there is no external force detected, confirming the durability of the force sensor. The cost of the sensor and continuum robots are listed in Table I, with a total cost of $7.6 and $75, respectively.

According to the predefined force detection range (0–3 N in the vertical direction and 0–0.5 N in the horizontal direction), we applied finite element analysis (FEA) in SolidWorks 2020 to simulate the maximum force in the x-, y-, and z-directions separately, and 1.5 mm thickness design matches the working range better than others. In Fig. 3(a)–(c), modes of bending under different external forces are illustrated. When the sensor is only subjected to the force in the z-direction, it will bend evenly in the three directions. When the sensor is pressed from the y-direction, one side of the tripod structure moves down in the z-direction while the other two sides move up. For the Fx pressure, one side is down, one side is up, and one side is twisted with small deflections in the z-direction. Fig. 3(d)–(f) further shows the FEA results of the 1.5 mm design. The simulated maximum force in the x, y, and z is 0.88, 0.65, and 3.88 N, respectively.

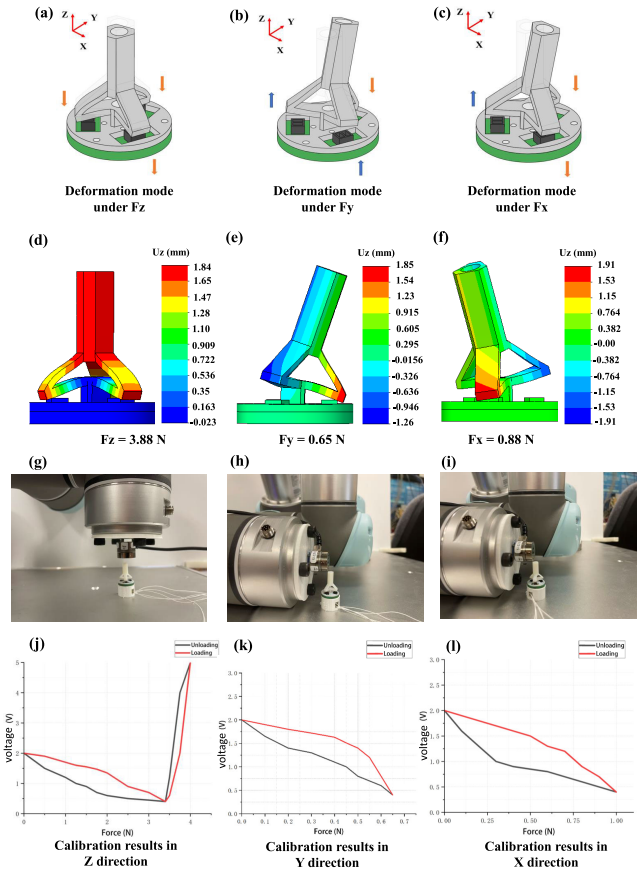

Fig. 3. Illustration of bending modes. (a)–(c) Deformation mode under pressures from z-, y-, and x-directions, respectively. (d)–(f) FEA results of the corresponding maximum force. (g)–(i) Calibration experiment. (j)–(l) Relationship of the loading and unloading process from calibration experiments.

Meanwhile, we used a commercial force sensor (ATI Nano 17) mounted on a UR5 robotic arm [in Fig. 3(g)–(i)] to show the relationship between force and voltage readings from optoelectronic sensors as well as maximum loading. For the test process, the robotics arm is positioned in defined x-, y-, and z-directions and set to 0.5 mm in a single moving step. When the readings from the commercial force sensor and optoelectronic sensors are stable, we record and move to the next step. If we observe that one side of the tripod sensor touches the optoelectronic sensor, the robotic arm will be stopped moving forward and then move back to the original position. Therefore, we define and record the maximum loading in x, y, and z, respectively (1, 0.65, and 3.88 N) as shown in Fig. 3(d)–(f). It is worth noting that due to the hysteresis of the material, the loading and unloading curves are different. Unlike traditional force sensors, this structure generates different deformation variables when the direction of force changes, resulting in the predicted value of the force sensor being related to the distance from the previous moment. Therefore, it is difficult to directly use the force and voltage curves as a calibrated result to predict real force in clinical use with traditional methods. Besides, as the vertical pressure can cause the side of the tripod structure to get closer to the optoelectronic sensor, the steep linear section of the sensor [Fig. 1(e)] is activated. While for forces in x- and y-directions, it is difficult to observe such a phenomenon. If the resultant force is applied to the gripper, for instance, $Fz + Fy$, it can

be confused which force versus voltage curves in Fig. 3(j)–(l) should be selected. We can conclude from experiments that the different force versus voltage curves under different external stimuli and hysteresis can make the traditional calibration method fail to predict real forces. Therefore, it is difficult to directly use the value of the instantaneous reading of the sensor to predict the size of the force. It is necessary to introduce more quantities that can describe the process of performing medical tasks to train.

The angle of the motor and the moving distance of the slide table can become the other three variables that describe the relative position of the continuum robot system. The two servos provide the degrees of freedom in the x- and y-directions and the slide table provides the degrees of freedom in the Z-direction. Through the prediction of the angle quantity, the deep neural network can be used to fit its movement process to conform to the force curve of loading and unloading, eliminate errors caused by assembly errors and friction in the robot system, and provide the direction of judgment force.

C. Implementation and Setup

In the implementation phase, we completed the neural network training of the force sensing prediction for four different surgical tools and corresponding clinical tasks. In terms of hardware setup, as shown in Fig. 4, the commercial force sensor (ATI-Nano 17) will be fixed with different artificial phantoms and connected with an NI data acquisition card to obtain the ground truth values. The frequency of sampling is set to 60 Hz for the commercial sensor to ensure a quick response from the ground truth side. The voltage values of the optoelectronic sensors are recorded by the microcontroller (Arduino Mega 2560) at the same frequency as the commercial force sensor. Simultaneously, the turning angle of the two servo motors and the moving displacement of the linear slider is recorded as well. The endoscope at the end of the robotics system is used to observe the state of the working tool and experiment phantom. Once the unpredicted behaviors occur in the process, the operators can stop the system and restart for another epoch of data collection. In terms of the manufacture of the artificial phantom, the oral cavity with the outstanding shape of the pharyngeal wall and tonsil is 3-D-printed first, then we pour a layer of silica gel made of Eco-flex 0010 with a thickness of 4 mm to mimic the soft tissues in the oral cavity. The phantom used in needle and microneedle insertion experiments is in the shape of a cylinder where the Eco-flex 0010 is poured into for curing. The palpation experiments use the same oral cavity phantom, which contains soft tissues and hard bones. For the tool selection in four different medical scenarios, a 1.5 mm hole is provided on the top of the soft gripper, and the interference fit between the rod and the hole is used for the fixation of cotton swabs, micro-needles, palpation probes, and needles. A 1.5 mm diameter rigid rod is used to hold all four tools.

Since our force prediction tasks are nonlinear and hysteresis, we proposed four learning methods to compare the advantages and disadvantages of handling different medical processes and select the relatively outperformed learning method to carry out further experiments. The four learning methods include

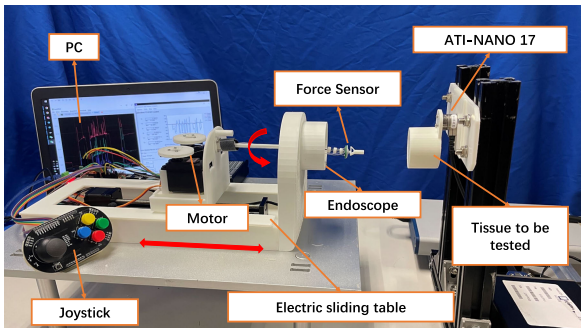

Fig. 4. Schematic of the experiment.

feedforward neural network (FNN), gate recurrent unit (GRU), long and short-term memory network (LSTM), and bidirectional LSTM (BiLSTM), where the FNN represents the normal fully connected neural network type and the rest three types of networks can be classified into an RNN. In general, each learning methods have its own features in regression tasks. FNN provides the direct fitting approach for a nonlinear relationship, but it can cause overfitting if the hidden neurons or layers are set to an excessive number. RNN solves regression problems with time series data, and the former information will be used for future predictions. By controlling the gated state, LSTM can remember the information that needs to be memorized for a long time and forget the unimportant information. Unlike naive RNN, which has only one way of memory superposition, LSTM is especially suitable for "long-term memory" tasks. GRU decreases a gated unit and also the tuning parameter, which leads to lower computational costs. The input of BiLSTM flows in both directions, utilizing information from both sides. This brings higher accuracy for time series regression.

To select the outperformed neural network for further validation experiments, we deployed the following four medical tasks to collect the training data. The detailed pipelines are listed as follows.

1) *Oralpharyngeal Sample Collection:* Because mimic pharyngeal tonsils on both sides are exposed, we will directly move the slider in the forward direction and then position the swab to one side of the pharyngeal tonsils. Then, the cotton swab is wiped back and forth slightly at least three times. After that, we will adjust the position of the swab to wipe the posterior pharyngeal wall up and down at least three times. Finally, repeat the same swabbing process for 10 min (20 512 data points).
2) *Percutaneous Needle Insertion:* We select 30° as the insertion angle between the soft tissue and needle, and then adjust the rotating angle of servo motors according to the kinematics of continuum robot as described in (2) and (3). After that, the angle of the motor will be fixed, and we use the linear slider to complete the percutaneous by moving forward and backward at a distance of 10 mm. Finally, repeat the same operation flow in other insertion positions on soft tissue for 6 min (12 307 data points).
3) *Microneedle for Drug Delivery:* We deliver the tip of the microneedle to the surface of the tissue by moving

TABLE II
RESULT OF TRAINING DATASET OF CORRESPONDING MEDICAL TASKS ON FOUR NEURAL NETWORKS

Medical task	Network	RMSE of Fx (mN)	NRMSE of Fx	RMSE of Fy (mN)	NRMSE of Fy	RMSE of FZ (mN)	NRMSE of Fz	Execution time per data point (ms)
Oralpharyngeal sample collection	FNN	0.0144	13.3%	0.0138	12.8%	0.0167	20.8%	0.009
	LSTM	0.0167	15.4%	0.0153	13.9%	0.0126	15.8%	0.006
	GRU	0.0126	11.6%	0.0126	11.4%	0.0157	19.6%	0.005
	BiLSTM	0.0182	16.6%	0.0147	13.3%	0.0164	20.5%	0.010
Percutaneous	FNN	0.0161	6.1%	0.0332	6.6%	0.0734	5.9%	0.012
	LSTM	0.0237	8.8%	0.0442	8.8%	0.0985	8.0%	0.006
	GRU	0.0202	7.7%	0.0391	7.8%	0.0958	7.7%	0.004
	BiLSTM	0.0207	7.7%	0.0459	8.0%	0.1114	9.1%	0.006
Microneedle for drug delivery	FNN	0.0339	15.0%	0.0238	13.5%	0.0531	7.5%	0.007
	LSTM	0.0212	9.5%	0.0420	24.7%	0.0676	9.5%	0.004
	GRU	0.0852	36.3%	0.0649	37.6%	0.0227	3.1%	0.005
	BiLSTM	0.0128	5.4%	0.0153	8.8%	0.0314	4.4%	0.009
Palpation of oral cavity	FNN	0.0628	12.0%	0.0114	13.8%	0.3750	11.3%	0.011
	LSTM	0.0682	13.6%	0.0090	11.2%	0.2851	8.6%	0.005
	GRU	0.0724	14.4%	0.0117	13.8%	0.3056	9.2%	0.005
	BiLSTM	0.0592	11.8%	0.0091	11.2%	0.2764	8.3%	0.012

the slider forward. As the length of microneedle tips is 1 mm, we move the slider forward again in 1 mm. Then, to verify and complete the drug release, the yaw angle of the tip will be slightly swung within a range of 10°. Finally, the same operation flow will be repeated for 8 min (16 410 data points).

4) *Palpation of the Oral Cavity:* We first select the position where soft tissues are covered and then move the slider 10 mm. Afterward, we select the hard bone position and repeat the same moving distance. Lastly, we repeat the above flows alternatively for 6.5 min (13 333 data points).

The pipeline of neural network training for the described four algorithms is comparable despite slight differences in parameters such as the number of hidden units and maximum training epochs. For FNN, the number of layers is set to 1 with 100 hidden units of neurons after GridSearch, and the number of maximum epochs is set to 1000. The network training function that updates weight and bias values is based on the Levenberg–Marquardt optimization algorithm. For RNN-type networks (LSTM, GRU, and BiLSTM), we use GridSearch to find the best hyperparameters, and the Adam optimizer is used with an initial learning rate of 0.01. We have used the Adam optimizer with an initial learning rate of 0.01 and introduced a dropout rate of 0.1 after 200 epochs to prevent overfitting. We have also normalized the readings of the photoelectric sensor to narrow the range of eigenvalues and mitigate the risk of overfitting. The Minibatch size is set to 64. Then, fewer training epochs (700) and the number of neurons (10) for one layer structure network are used. The configuration of the mentioned neural network uses using the library in MATLAB. In this work, we will use root mean square error (RMSE), and the relative normalized RMSE (NRMSE) to compare different networks as shown in Table II. We use mean squared error (MSE) as the loss function to evaluate the model performance

$$\text{Loss} = \frac{1}{N}\sum_{i=1}^{N}\left(\hat{F}_i - F_i\right)^2$$

where N is the number of samples, F_i is the true output value of the ith sample, and $\hat{F}_i$ is the predicted output value of the ith sample.

In terms of different interventional tasks, the performance of the test network is different. However, setting up reliable criteria from the results we obtained is essential for future validation experiments as well as real applications. The selected criteria include accuracy, time cost, the standard deviation of errors on different force directions, outliers, and the number of the input sequence (see Table III). It can be seen that networks applied in percutaneous are more precise than others because it has a simple movement pattern. For different applications, we need to find out the prior known weights of the force range in x, y, and z. If the force in one direction during the specific task has no contribution to the resultant force, which can be considered as noises around 0 N. Therefore, for the microneedle drug delivery process, the Fy obviously only fluctuated around 0 N within a small and irregular force range. Except for absolute accuracy, the NRMSE difference between weighted Fx, Fy, and Fz cannot be large. For example, the GRU network in microneedles for drug delivery experiments has an NRMSE difference at 33.2% between Fx and Fz. Compared to the FNN network, the RNN-type network can have advantages in avoiding overfitting with a small number of neurons, which can improve computational efficiency as well. For BiLSTM, because it requires both sides of data as a minibatch to predict the force, the time delay can occur when we consider the real application. Therefore, by comparing the features and accuracy of the above neural network, we will select the LSTM network for the experimental stage and further applications.

III. EXPERIMENTS AND RESULTS

In this section, we carry out the validation experiments of all the predescribed medical tasks. As shown in Fig. 4, when the medical staff performs a specific medical task, the robotic system is simply controlled by a joystick. As a typical human-in-loop system, the endoscope can provide guidance

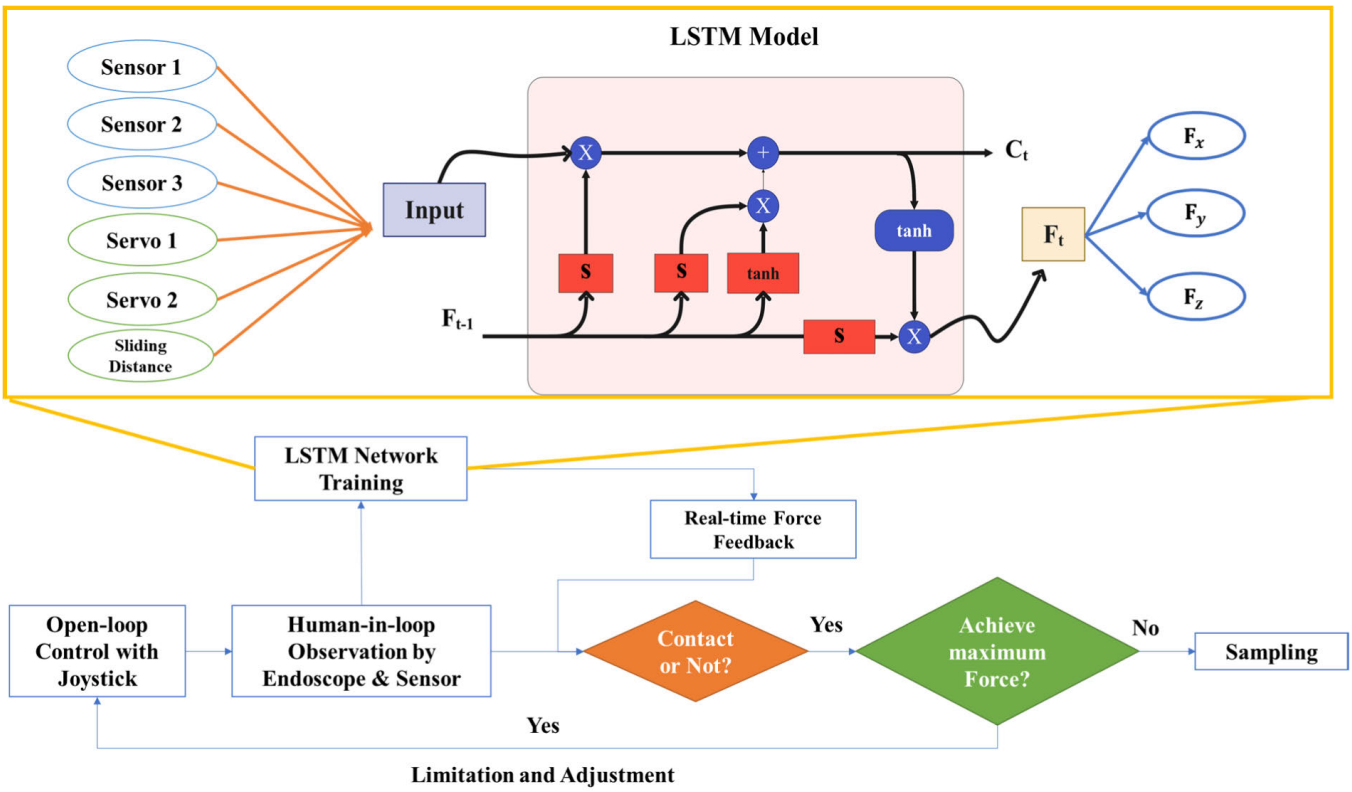

Fig. 5. LSTM neural network structure and control loop diagram of the system.

TABLE III
EVALUATIONS ON DIFFERENT NEURAL NETWORKS

Neural network	Max. Std. of NRMSE	Outlier	Input sequence	Time cost ranking
FNN	3.66%	✓	1 data point	4^{th}
LSTM	1.91%	✗	64 data points (t_-)	2^{nd}
GRU	16.60%	✗	64 data points (t_-)	1^{st}
BiLSTM	2.94%	✗	64 data points (t_+ and t_-)	3^{rd}

for positioning and navigation for operators. The pretrained LSTM network for a specific task is included for real-time force-sensing feedback to the computer screen. The angle of the servo motors and the displacement of the slide indicates the position of the continuous robot under the constant curvature model, which makes the system more robust. To avoid outliers generated by the signals received by the photoelectric switch, we use the mean filter to process the readings of the three optoelectronic sensors and conduct normalization processing in the subsequent training to obtain more obvious input characteristics. Three voltage signals from optoelectronic sensors are highly sensitive and in real-time, and the network will make predictions for forces in the three directions of xyz by combing two types of input information. Simultaneously, the contact sign and safety valve are set in parallel to ensure the operation is effective and safe. In terms of contact condition, the variations in three directions are defined as contact signs. For the safety valve, the maximum endurance for the z-direction is set to 4 N, while forces in the x- and y-directions are set to 1 N. By following the control framework in Fig. 5, we will perform the validation experiments for medical applications. Besides,

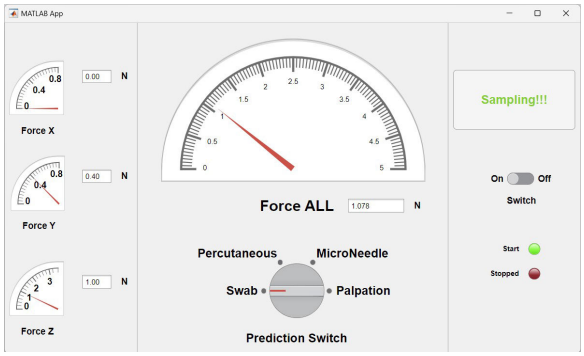

Fig. 6. User-friendly graphical interface for the force sensing system.

we used MATLAB to make a GUI interface for real-time prediction of force values in Fig. 6 to better control with human-in-loop. This interface can display the forces in the three directions of x, y, and z, respectively, and output the resultant force in the interface. If the force is too large during use, an early warning will be issued on the right side, and the emergency stop will return to the original position after reaching the maximum range. This design ensures the safety of the human tissue to be tested and can better control the equipment.

A. Case I: Oral Swabbing Force Sensing Robotics System

The recent Covid-19 pandemic requires a large amount of oral or nasopharyngeal swabbing to test if people are at high risk of spreading the virus or not. Compared to complicated nasopharyngeal swabbing, oral cavity swabbing has advantages in safety, easy operation, and high comfort level. Nevertheless, as a repeatable medical task, it is crucial

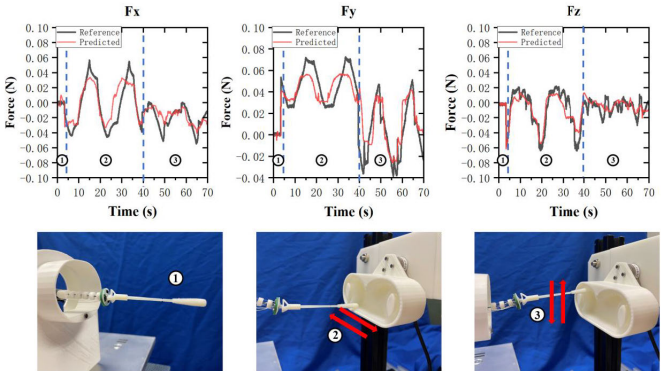

Fig. 7. Oral cavity swab experiment. Stage 1: preparation. Stage 2: swab the epiglottis from left to right in x-direction (repeated twice). Stage 3: swab the epiglottis upside down (repeated twice).

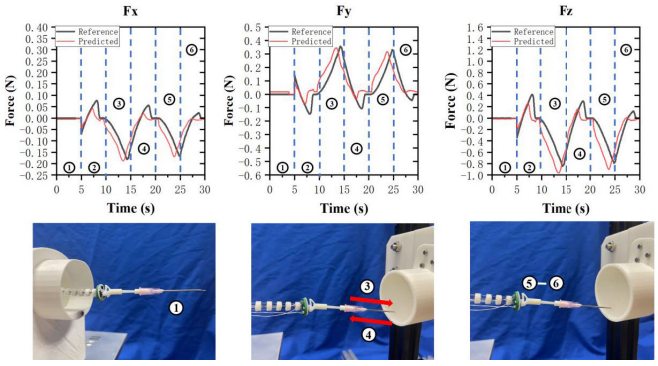

Fig. 8. Needle insertion experiment at an angle of 30°. Stage 1: preparation. Stage 2: moving the tip of the needle to the specific angle and place. Stage 3: insertion for 3 s. Stage 4: retraction for 4 s. Stages 5 and 6: repeat insertion and retraction process at the same place.

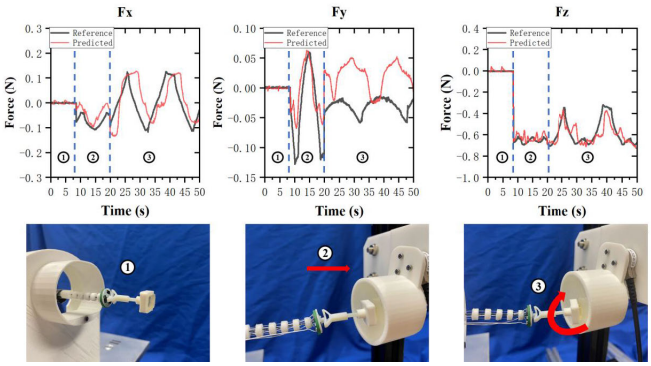

Fig. 9. Microneedle insertion experiment. Stage 1: preparation. Stage 2: moving the slider forward to make contact with soft tissue. Stage 3: rotating the microneedle in x-direction to test that the insertion (stage 2) is successful (repeated twice).

that sampling positions, including posterior pharyngeal wall and tonsil, have been fully contacted with cotton swabs to obtain effective samples for further polymerase chain reaction (PCR) tests [24]. Such a process relies on the experience and subjective perception of clinical operators who are usually under temporary training, which can cause the sample in poor quality or uncomfortable feelings for patients. Therefore, using accurate 3-D force information to monitor the swabbing task is a significant approach to address the abovementioned issues.

During the sampling process, as shown in Fig. 7, we swipe the cotton swab right and left in the tonsil area in stage 2. It shows that the tip of the swab is under fluctuated Fx from -0.04 to 0.06 N, positive Fy ranging from 0.03 to 0.07 N, and negative maximum Fz at 0.06 N. When we take the sample in the posterior pharyngeal wall, it is clear that the swab is mainly under pressure from Fy and Fx. The NRMSE for Fx, Fy, and Fz are 16.1%, 13.5%, and 15.4%. Except for the ordinary vibration at stage 3 in the Fz graph and delays in Fy at stage 2, the sampling process is monitored by providing force information with an accuracy of more than 85%.

B. Case II: Soft Tissue Percutaneous Force Sensing Robotics System

Soft tissue percutaneous is a procedure widely used minimally invasive intervention to achieve tasks such as blood sampling, tool placement, and drug delivery. When we perform human soft tissue percutaneous in vivo tasks, we can usually monitor the process and learn the relevant information only under the guidance of imaging technology (ultrasound and CT) [25], [26]. Thus, exploring a simple and direct way to detect the insertion state while maintaining the surveillance of contact force between the needle and tissues can be useful in practical applications.

In this article, we employed force data sensed in this study and divided the entire process into different stages (start, contact, insertion, retraction, and repetition.) according to the Fx, Fy, and Fz performance. As shown in Fig. 8, in the process of stages 1–6, medical staff can clearly identify the current status of soft tissue percutaneous and use a continuum robot to operate and obtain real-time force contact information, which will provide more help for real-time force feedback of soft tissue percutaneous. In the process of 2–3 and 4–5, the needle pierced the soft tissue made of Ecoflex 00-10 at a 30°, and the distribution of xyz value at the time of insertion can be clearly seen. The direction of the force changes because during the insertion and extraction process, the direction of the interaction force between the needle and the tissue is opposite, and the peak value of 1 N in the z-direction is reached. At the same time, compared with the training data set, the NRMSE of Fx, Fy, and Fz in this task are 9.2%, 9.1%, and 8.0%.

C. Case III: Microneedle Insertion Force Sensing Robotics System

As a rapidly developing medical technology, microneedle gains advantages in painless treatment and quick recovery. Systemic administration can be trivial and less efficient compared to microneedle drug delivery. However, the microneedle delivery process often requires some high-precision microscopic images to detect whether the process is completed and the information of insertion depth [27]. This is very troublesome and expensive. If we use 3-D force information to achieve or replace the same or part of functions, it will bring enlightenment to the field of microneedle drug delivery.

As shown in Fig. 9, the system has adopted a new operation procedure for microneedles. When microneedles need to deliver drugs to tissues in specific parts of the inside human body, it is necessary to obtain real-time force feedback from tissues. As shown in stage 2, when the microneedle contacts

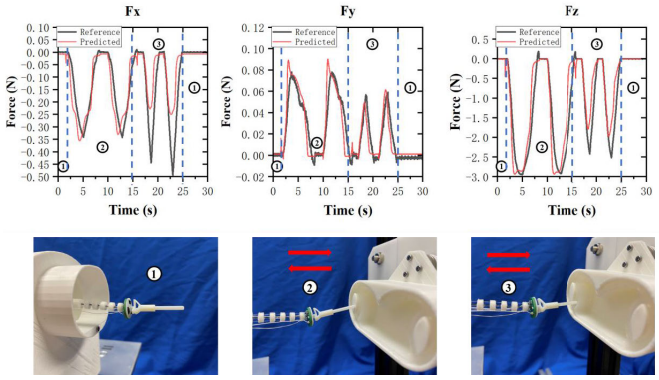

Fig. 10. Palpation experiment. Stage 1: preparation. Stage 2: move the slider in a straight line to touch the artificial hard tissue (repeated twice). Stage 3: move the slider in a straight line to touch the artificial soft tissue (repeated twice).

the tissue, the force in the z-direction reaches 0.8 N and a significant change occurs, indicating that the tissue has been contacted with the microneedle. In stage 3, we use the continuum robot to behave in the yaw direction while the contact point in the z-direction of the microneedle is unchanged. To verify that the drug to the tissue is completed, we can see that a micro force range within 0.1 N is appeared up and down, which also shows that the contact is safe. It can be noted that there is an obviously unpredictable range in Fy at stage 3, which is due to there being no force in that direction and noises of commercial sensors influencing the behavior of the force curve. Except that, the NRMSE of Fx and Fz is 9.2% and 9.4%, respectively. This method can better complete the application of all areas, providing us with a better microneedle delivery solution.

D. Case IV: Palpation Force Sensing Robotics System

As a contact diagnostic method, palpation is often used by doctors to detect and diagnose tissues [28]. For ex vivo situations, performing palpation is direct and simple by using any force sensor or proprioception of doctors. Xiao et al. [29] used a UR5 robotic manipulator with a commercial force sensor mounted as the end-effector as the hardware setup for depth estimation during tissue palpation. However, for in vivo tasks, it is inevitable to use a continuum robot/equipment to perform diagnosis, and the obstacles are proprioception cannot be used. The traditional force sensor cannot be integrated into the near tip side of the robot to obtain more accurate force information for palpation. Therefore, we apply a self-designed robot to perform palpation tasks inside the deep of the oral cavity and predict the force in real-time.

As shown in Fig. 10, when such a hard probe contacts tissues with different hardness at a certain angle, Ecoflex 00-10 and PLA are used for comparison in this experiment. After the slider moves the same distance, the magnitude of x, y, and z of the force generated is obviously different, where Fz weighted more than Fx and Fy. Medical operators can easily distinguish the magnitude of force values in stages 2 and 3 of tissues with different hardness. The extreme values in the Z-direction are 2 and 3 N, respectively. The NRMSE for Fx, Fy, and Fz are 14%, 11.1%, and 9.2%. This method provides a possibility for a remote surgical palpation system.

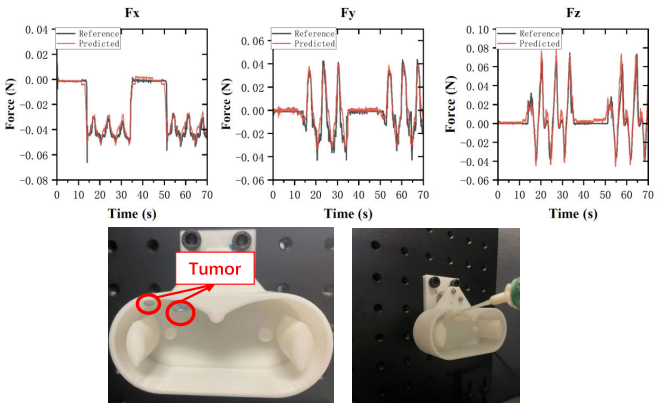

Fig. 11. Swab experiment with different oral cavities and tumor existing environment.

E. Case V: Oral Swabbing Force Sensing Robotics System With Environmental Noise

After conducting four application tests, the continuum robot system utilizing the RNN-LSTM network has been proven to complete various medical tasks on human tissues with excellent performance and safety. To further enhance the model's robustness and generalization, we conducted tests using a variety of noisy environments to evaluate sensor performance. In the experiment, we replaced the original Ecoflex 00-10 substrate with a more rigid substrate. We used different mouth sizes to fit multiple groups of neural networks representing oral compositions at different ages, ensuring better swab robustness. In addition, we fixed a soft plasticine tumor on the rigid substrate to simulate the soft tissue of the human body, which may produce noise when the force sensor receives data. We collected nine datasets with different combinations in three oral cavity types and on a PLA rigid substrate at speeds of 0.05, 0.25, and 0.50 mm/s and evaluated them as a test set at 0.7 mm/s. As shown in Fig. 11, the NRMSE of Fx, Fy, and Fz were found to be 7.75%, 6.92%, and 9.57%, respectively. The training set's performance across multiple environments demonstrated the network's robustness and generalization in complex human tissue environments. Our study confirms the suitability of the network to complete varied medical tasks safely.

IV. Conclusion

A miniaturized and affordable micro force sensing system enhanced by deep learning algorithms is proposed. It can be employed to estimate the interaction force of the distal end of continuum robot and achieve interventional phase identification in the specific robot-assisted interventional procedure. Such a force sensing system is designed and fabricated with a 3-D-printed soft sensor mounted on our developed continuum robotic platform to grip various end-effector instruments. Due to its compliance and flexibility, potential harm to human tissues caused by rigid contact can be eliminated. In addition, optoelectronic sensors are sensitive to small variations of distances, which also utilize the softness of the selected material of the force sensor. The sensor ingeniously converts the force value information transmitted by the object's constitution into more accurate distance information. It uses

various provided by the test bench to perform accurate fitting using the RNN-LSTM network to eliminate nonlinear and inherent errors, including friction, assembly tolerance, and hysteresis. For different medical tasks, such as oropharyngeal sample collection, percutaneous, microneedle administration, and palpation of the oral cavity, our method is used to predict force with high precision of more than 85%, a small measuring range under 0.1 N, and fast response speed within 0.2 s. The maximum force range of the system is set to 0–3.88 N in the z-direction, 0–0.65 N in the y-direction, and 0–1 N in the x-direction according to FEA simulation and experimental calibration. By designing several groups of neural networks (FNN, LSTM, GRU, and BiLSTM) fitting test experiments among different medical tasks, we compared the training results concerning accuracy for proposed neural networks. It shows that for different medical tasks and different force directions, the accuracy of each neural network varies. Therefore, when we select one network for further validation or even future application, we need to consider factors such as execution time cost, computational training cost, real-time performance, and the possibility of overfitting. The RNN-LSTM network is selected based on its advantages in mentioned aspects. The results of validation experiments show that the force sensing system we designed can complete the force estimation of tissue contact with shallow errors. This test method can effectively eliminate the errors caused by the hysteresis effect of the continuum and materials. The printed sensor can achieve the same effect as the commercial high-precision sensor accurately and significantly reduce the production cost, which can be effectively applied to large-scale medical system deployment. Finally, to overcome the shortcomings of less robustness of the RNN-LSTM network, we conducted oropharyngeal swab sampling experiments as an example and resampled the data under different oral tolerance and sampling speed. The data were then mixed together and retrained, which greatly improved the precision of the predictions.

Although the system has extremely high accuracy and response speed, at the same time, it also has some defects. For example, the size of the sensor can be further reduced and the bending effect of the material structure used can be more stable. In the future, we will focus on the integration and miniaturization of the system, so as to obtain a more intelligent, effective, and convenient medical force feedback system.

REFERENCES

[1] P. E. Dupont et al., "A decade retrospective of medical robotics research from 2010 to 2020," *Sci. Robot.*, vol. 6, no. 60, Nov. 2021, Art. no. eabi8017.

[2] S. Wang, K. Wang, R. Tang, J. Qiao, H. Liu, and Z. Hou, "Design of a low-cost miniature robot to assist the COVID-19 nasopharyngeal swab sampling," *IEEE Trans. Med. Robot. Bionics*, vol. 3, no. 1, pp. 289–293, Feb. 2021.

[3] F. Sun, J. Ma, T. Liu, H. Liu, and B. Fang, "Autonomous oropharyngeal-swab robot system for COVID-19 pandemic," *IEEE Trans. Autom. Sci. Eng.*, early access, Sep. 23, 2022, doi: 10.1109/TASE.2022.3207194.

[4] A. Gao, N. Liu, M. Shen, M. E. M. K. Abdelaziz, B. Temelkuran, and G.-Z. Yang, "Laser-profiled continuum robot with integrated tension sensing for simultaneous shape and tip force estimation," *Soft Robot.*, vol. 7, no. 4, pp. 421–443, Aug. 2020.

[5] T. O. Akinyemi et al., "Fiber Bragg grating-based force sensing in robot-assisted cardiac interventions: A review," *IEEE Sensors J.*, vol. 21, no. 9, pp. 10317–10331, May 2021.

[6] A. Gijbels, E. B. Vander Poorten, P. Stalmans, and D. Reynaerts, "Development and experimental validation of a force sensing needle for robotically assisted retinal vein cannulations," in *Proc. IEEE Int. Conf. Robot. Autom. (ICRA)*, May 2015, pp. 2270–2276.

[7] Z. Chua, A. M. Jarc, and A. M. Okamura, "Toward force estimation in robot-assisted surgery using deep learning with vision and robot state," in *Proc. IEEE Int. Conf. Robot. Autom. (ICRA)*, May 2021, pp. 12335–12341.

[8] S. Grazioso, G. Di Gironimo, and B. Siciliano, "A geometrically exact model for soft continuum robots: The finite element deformation space formulation," *Soft Robot.*, vol. 6, no. 6, pp. 790–811, Dec. 2019.

[9] N. Bandari, J. Dargahi, and M. Packirisamy, "Miniaturized optical force sensor for minimally invasive surgery with learning-based nonlinear calibration," *IEEE Sensors J.*, vol. 20, no. 7, pp. 3579–3592, Apr. 2020.

[10] K. Chin, T. Hellebrekers, and C. Majidi, "Machine learning for soft robotic sensing and control," *Adv. Intell. Syst.*, vol. 2, no. 6, Jun. 2020, Art. no. 1900171.

[11] J. Hu et al., "Flexible six-dimensional force sensor inspired by the tenon-and-mortise structure of ancient Chinese architecture for orthodontics," *Nano Energy*, vol. 96, Jun. 2022, Art. no. 107073.

[12] B. Fang, Z. Xia, F. Sun, Y. Yang, H. Liu, and C. Fang, "Soft magnetic fingertip with particle-jamming structure for tactile perception and grasping," *IEEE Trans. Ind. Electron.*, vol. 70, no. 6, pp. 6027–6035, Jun. 2023.

[13] Y. Guo, B. Pan, Y. Fu, and M. Q.-H. Meng, "CAM-FoC: A high accuracy lightweight deep neural network for grip force measurement of elongated surgical instrument," *IEEE Trans. Instrum. Meas.*, vol. 70, pp. 1–12, 2021.

[14] T. G. Thuruthel, B. Shih, C. Laschi, and M. T. Tolley, "Soft robot perception using embedded soft sensors and recurrent neural networks," *Sci. Robot.*, vol. 4, no. 26, Jan. 2019, Art. no. eaav1488.

[15] F. Wan, X. Liu, N. Guo, X. Han, F. Tian, and C. Song, "Visual learning towards soft robot force control using a 3D metamaterial with differential stiffness," in *Proc. Conf. Robot Learn.*, 2022, pp. 1269–1278.

[16] Z. Sun, Z. Wang, and S. J. Phee, "Elongation modeling and compensation for the flexible tendon-sheath system," *IEEE/ASME Trans. Mechatronics*, vol. 19, no. 4, pp. 1243–1250, Aug. 2014.

[17] D. C. Rucker and R. J. Webster, "Deflection-based force sensing for continuum robots: A probabilistic approach," *Proc. IEEE/RSJ Int. Conf. Intell. Robots Syst.*, Sep. 2011, pp. 3764–3769.

[18] M. Khoshnam, A. C. Skanes, and R. V. Patel, "Modeling and estimation of tip contact force for steerable ablation catheters," *IEEE Trans. Biomed. Eng.*, vol. 62, no. 5, pp. 1404–1415, May 2015.

[19] L. Massari et al., "A machine-learning-based approach to solve both contact location and force in soft material tactile sensors," *Soft Robot.*, vol. 7, no. 4, pp. 409–420, Aug. 2020.

[20] T. Li, N. K. K. King, and H. Ren, "Disposable FBG-based tridirectional force/torque sensor for aspiration instruments in neurosurgery," *IEEE Trans. Ind. Electron.*, vol. 67, no. 4, pp. 3236–3247, Apr. 2020.

[21] J. Li, C. Wang, Z. Mao, Y. Liu, Z. Wang, and H. Liu, "A compact FBG-based triaxial force sensor with parallel helical beams for robotic-assisted surgery," *IEEE Trans. Instrum. Meas.*, vol. 71, pp. 1–9, 2022.

[22] H. Wang, Z. Yan, Y. Gao, W. Wang, and Z. Du, "3-D force sensing strategy of laryngeal continuum surgical robot based on fiber Bragg gratings," *IEEE Trans. Instrum. Meas.*, vol. 70, pp. 1–10, 2021.

[23] F. Feng, W. Hong, and L. Xie, "A learning-based tip contact force estimation method for tendon-driven continuum manipulator," *Sci. Rep.*, vol. 11, no. 1, pp. 1–11, Sep. 2021.

[24] I. Floriano, A. Silvinato, W. M. Bernardo, J. C. Reis, and G. Soledade, "Accuracy of the polymerase chain reaction (PCR) test in the diagnosis of acute respiratory syndrome due to coronavirus: A systematic review and meta-analysis," *Revista da Associação Médica Brasileira*, vol. 66, no. 7, pp. 880–888, Jul. 2020.

[25] S. Chen, Y. Lin, Z. Li, F. Wang, and Q. Cao, "Automatic and accurate needle detection in 2D ultrasound during robot-assisted needle insertion process," *Int. J. Comput. Assist. Radiol. Surgery*, vol. 17, no. 2, pp. 295–303, Feb. 2022.

[26] É. Dorileo, N. Zemiti, S. Krut, and P. Poignet, "CT/MR-compatible physical human–robotized needle interactions: From modeling to percutaneous steering," *Mechatronics*, vol. 85, Aug. 2022, Art. no. 102840.

[27] J. Enfield, M.-L. O'Connell, K. Lawlor, E. Jonathan, C. O'Mahony, and M. Leahy, "In-vivo dynamic characterization of microneedle skin penetration using optical coherence tomography," *J. Biomed. Opt.*, vol. 15, no. 4, 2010, Art. no. 046001.

[28] Z. Zhou et al., "Methods to recognize depth of hard inclusions in soft tissue using ordinal classification for robotic palpation," *IEEE Trans. Instrum. Meas.*, vol. 71, pp. 1–12, 2022.

[29] B. Xiao et al., "Depth estimation of hard inclusions in soft tissue by autonomous robotic palpation using deep recurrent neural network," *IEEE Trans. Autom. Sci. Eng.*, vol. 17, no. 4, pp. 1791–1799, Oct. 2020.

Shilong Yao received the B.E. degree in mechanical engineering from the Southern University of Science and Technology, Shenzhen, China, in 2021. He is currently pursuing the Ph.D. degree with the Department of Electrical Engineering, City University of Hong Kong (CityU), Hong Kong.

His current research interests include soft robotics, sensing, control, and robot learning in medical robotic systems.

Ruijie Tang received the joint B.S. degree in mechanical engineering from the South China University of Technology, Guangzhou, China, and the University of Edinburgh, Edinburgh, U.K., in 2018, and the M.S. degree in advanced aeronautical engineering from the Imperial College London, London, U.K., in 2019. He is currently pursing the Ph.D. degree in electronic engineering with The Chinese University of Hong Kong, Hong Kong.

His current research interests include soft robots, force sensor designs, and magnetically actuated robots with applications in the medical field.

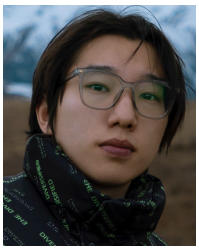

Long Bai received the B.S. degree in optoelectronics information science and engineering from the Beijing Institute of Technology (BIT), Beijing, China, in 2021. He is currently pursuing the Ph.D. degree with the Department of Electronic Engineering, The Chinese University of Hong Kong (CUHK), Hong Kong.

His current research interests include robotics perception, capsule endoscopy, surgical scene understanding, continual learning, and human–robot interaction.

Mr. Bai was a recipient of the CUHK Vice-Chancellor's Ph.D. Scholarship Scheme in 2021, the IEEE RAS Travel Grants Award in 2023, and the Best Poster Award in ICRA Workshop on Surgical Robotics in 2023.

Hong Yan (Fellow, IEEE) received the Ph.D. degree from Yale University, New Haven, CT, USA.

He was a Professor of imaging science with the University of Sydney, Camperdown, NSW, Australia. He is currently a Wong Chun Hong Professor of data engineering and a Chair Professor of computer engineering with the City University of Hong Kong, Hong Kong. His research interests include image processing, pattern recognition, and bioinformatics. He has authored or coauthored over 600 journals and conference papers in these areas.

Dr. Yan is an IAPR Fellow, a member of the European Academy of Sciences and Arts, and a fellow of the U.S. National Academy of Inventors. He received the 2016 Norbert Wiener Award for contributing to image and biomolecular pattern recognition techniques from the IEEE SMC Society.

Hongliang Ren (Senior Member, IEEE) received the Ph.D. degree in electronic engineering (specialized in biomedical engineering) from The Chinese University of Hong Kong (CUHK), Hong Kong, in 2008.

He has navigated his academic journey through CUHK; Johns Hopkins University, Baltimore, MD, USA; Children's Hospital Boston, Boston, MA, USA; the Harvard Medical School, Boston; Children's National Medical Center, Washington, DC, USA; and the National University of Singapore (NUS), Singapore. He is currently an Associate Professor with the Department of Electronic Engineering, CUHK, and an Adjunct Associate Professor with the Department of Biomedical Engineering, NUS. His research interests include biorobotics, intelligent control, medical mechatronics, soft continuum robots, soft sensors, and multisensory learning in medical robotics.

Dr. Ren was a recipient of the NUS Young Investigator Award, the Engineering Young Researcher Award, the IAMBE Early Career Award in 2018, the Interstellar Early Career Investigator Award in 2018, and the ICBHI Young Investigator Award in 2019. He serves as an Associate Editor for the IEEE TRANSACTIONS ON AUTOMATION SCIENCE AND ENGINEERING and the *Medical and Biological Engineering and Computing* (MBEC).

Li Liu (Member, IEEE) received the Ph.D. degree in biomedical engineering from the University of Bern, Bern, Switzerland.

He was a Post-Doctoral Fellow with the University of Bern and The Chinese University of Hong Kong (CUHK), Hong Kong. He has been an Assistant Professor with the School of Biomedical Engineering, Shenzhen University, Shenzhen, China, since 2016. In 2019, he joined CUHK as a Faculty Member. His current interests focus on the interface of surgical robotics, in situ sensing, and medical imaging, and to develop robotic-enabled medical imaging, as well as image-guided robotic surgical systems, where ultrasound, photoacoustic sensing/imaging, and endoscopic OCT are three major modalities to be investigated and incorporated with minimally invasive surgical robotics.

Dr. Liu served as the Program and Publication Chair for many international conferences, including the Publication Chair of IEEE ICIA 2017, 2018, the Program Chair of ROBIO 2019, and the Video Chair of IEEE ICRA 2021. He was a recipient of the Distinguished Doctorate Dissertation Award, the Swiss Institute of Computer Assisted Surgery in 2016, the MICCAI Student Travel Award in 2014, and the Best Paper Award of IEEE ICIA in 2009. He has been an Associate Editor of *Biomimetic Intelligence and Robotics* (BIROB) since 2021.